RSC Advances

ROYAL SOCIETY OF CHEMISTRY

www.rsc.org/advances

Graphical Abstract

CeO_2-decorated Ni/γ-Al_2O_3 exhibited high activity, coking- and sintering-resistance for CO methanation because CeO_2 selectively deposited on the surface of NiO.

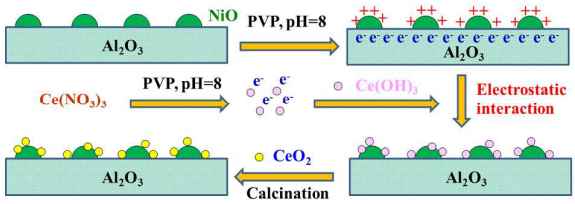

Highly active and stable Ni/γ-Al_2O_3 catalysts selectively deposited with CeO_2 for CO methanation

Qing Liu,[a] Jiajian Gao,[a] Meiju Zhang,[a] Huifang Li,[a] Fangna Gu,[a,*]

Guangwen Xu,[a] Ziyi Zhong,[b] and Fabing Su[a,*]

[a] *State Key Laboratory of Multiphase Complex Systems, Institute of Process Engineering, Chinese Academy of Sciences, Beijing, China 100190*

[b] *Institute of Chemical Engineering and Sciences, A*star, 1 Pesek Road, Jurong Island, Singapore 627833*

*Corresponding author. Tel.: +86 10 82544850; fax: +86 10 82544851. *E-mail address:* fngu@ipe.ac.cn (F. Gu); fbsu@ipe.ac.cn (F. Su).

Abstract

We report the preparation of highly active, coking- and sintering-resistant CeO_2-decorated Ni/γ-Al_2O_3 catalysts by impregnation method followed by a modified deposition-precipitation (DP) of CeO_2. The samples were characterized with Nitrogen adsorption, X-ray diffraction, scanning electron microscopy, transmission electron microscopy, thermogravimetric analysis, H_2 temperature-programmed reduction, H_2 temperature-programmed desorption and zeta potential analysis. The results revealed that compared with the Ni catalysts with a NiO loading of 40 wt% prepared by co-impregnation (CI) and sequential impregnation (SI) methods, the Ni catalyst synthesized by DP method showed the enhanced catalytic performance for CO methanation at atmospheric pressure and an extremely high weight hourly space velocity (WHSV) of 240000 mL g^{-1} h^{-1}. In a 50-h high-pressure life-test, this catalyst showed a high resistance to both coking and sintering. It was found that CeO_2 nanoparticles were selectively deposited on the surface of NiO rather than on Al_2O_3 due to the electrostatic interaction during the DP process, effectively restraining Ni particles from sintering during the reduction and reaction at the high temperatures, and inhibiting coke formation by increasing supply of active oxygen species on the nickel surface. As a result, the formed CeO_2-decorated Ni/Al_2O_3 catalyst exhibited excellent catalytic performance and stability in CO methanation. This work demonstrated that catalytic property could be much improved on a usual catalyst but with well-designed structure.

1. Introduction

The production of synthetic natural gas (SNG) via methanation reaction ($CO + H_2 \rightarrow CH_4 + H_2O$) is of great interest,[1, 2] particularly in the regions with rare natural gas and abundant coal resources such as China and Korea. Normally, coal or biomass can be gasified to produce synthesis gas containing CO and H_2, which can be used as the raw gases of methanation. In this reaction, Ni/Al_2O_3 catalysts are often employed due to their relatively high activity and low cost.[3] However, these catalysts often suffer from sintering of the Ni particles and the Al_2O_3 support as well as coke formation on Ni during the methanation process.[4, 5] In the last several decades, great efforts have been made to improve the Ni/Al_2O_3 catalysts, e.g., by modification of the Al_2O_3 support,[6] by application of various preparation methods including solution combustion method[7] and single-step sol-gel method,[8] and by use of various promoters such as MgO,[9] ZrO_2[10] and MnO_x.[11] Although partial success has been achieved, it is still hard to simultaneously inhibit the coke formation and sintering of Ni particles to obtain a high catalytic activity. Hence, the stability of Ni/Al_2O_3 catalyst should be further improved.

In heterogeneous catalysis, CeO_2 is often used as structural and electronic promoter or support, mainly because of its ability to improve dispersion of active components and thermal stability of the support, and to enhance the migration and exchange of oxygen species.[12, 13] For example, acting as the promoter of Ni/Al_2O_3 catalysts for CO and/or CO_2 methanation to increase the dispersion of Ni particles as well as their reducibility, thus to improve their catalytic activity.[14-16] However, coking- and sintering-resistant behaviors of the above catalysts in the methanation reaction are not yet investigated, particularly under the harsh reaction conditions such as high reaction temperatures and high weight hourly space velocities (WHSVs). Although coking and sintering often occur simultaneously, most of approaches can only work on one of them. Indeed, several Ni catalysts have

been reported to inhibit coking and sintering of Ni particles simultaneously while maintaining the high catalytic activity of the catalysts in methane reforming with carbon dioxide,[17-19] methanation of carbon monoxide,[20, 21] and other hydrocarbon reactions such as partial oxidation of methane to syngas.[22] There are still some limitations in the methods to synthesize these catalysts, including the use of expensive materials such as block copolymers[17] and organometallic salts,[17, 19] low NiO loadings,[20, 21] complicated preparation conditions,[22] and the need of special equipment such as atomic layer deposition reactor.[18] Therefore, it is necessary to develop new method to prepare Ni/Al_2O_3 catalyst with high resistance to coking and sintering.

Recently there are several reports showing that the construction of an oxide-on-metal surface structure, the so-called inverse catalysts, can enhance the catalytic reactivity of metal catalysts dramatically.[23-25] Inspired by the progress in catalyst development, we worked on a series catalysts that have specific oxide-on-metal structures. Following our previous work on CO methanation,[9, 20, 26-29] here we report CeO_2-decorated $Ni/\gamma\text{-}Al_2O_3$ catalysts with a NiO loading of 40 wt% for enhanced CO methanation. The $Ni/\gamma\text{-}Al_2O_3$ catalysts were prepared by impregnation method followed with addition of CeO_2 by a modified deposition-precipitation (DP) procedure, by which the CeO_2 particles were selectively deposited on NiO. The obtained catalyst is much more active than those prepared by co-impregnation (CI) and sequential impregnation (SI) methods, and is stable for CO methanation under the harsh reaction conditions. It is found that, in this DP-derived catalyst, two structural factors are responsible for the outstanding catalytic performance. First, the CeO_2 nanoparticles (NPs) are selectively deposit on the Ni surface and act as a physical barrier to restrain the growth of the Ni particles during the reduction and catalytic reaction at high temperatures; Second, the addition of CeO_2 can inhibit the growth of carbon filaments by increasing supply of active oxygen species on the Ni surface during the reaction.

2. Experimental

2.1. Catalyst preparation

All the chemicals of analytical grade including cerium (III) nitrate hexahydrate ($Ce(NO_3)_3 \cdot 6H_2O$), ammonia (NH_4OH), polyethylene glycol (PEG) (average molecular weight (MW) =20 000), nickel (II) nitrate hexahydrate ($Ni(NO_3)_2 \cdot 6H_2O$) and ethanol were purchased from Sinopharm Chemical Reagent Co. Ltd., China, and used without further treatment. Polyvinyl pyrrolidone (PVP) (MW=58,000) was purchased from Alfa Aesar. The commercial porous γ-Al_2O_3 (purity >95% GongYiHuaYu Alumina Co. Ltd., China) with a surface area of 300 m^2 g^{-1} was calcined at 400 °C in air for 2 h before use. The Ni/γ-Al_2O_3 catalyst was prepared by the wet impregnation method.Typically, 0.89 g of PEG and 7.79 g of $Ni(NO_3)_2 \cdot 6H_2O$ were dissolved in 50 mL deionized water, then 3.00 g of the γ-Al_2O_3 support was added to the above solution to form a slurry, which was kept vigorous stirring at room temperature overnight, and then heated to 80 ^oC to evaporate the liquid, dried at 100 ^oC for 24 h and further calcined at 400 ^oC for 2 h in air with the heating rate of 2 ^oC min^{-1}. The collected catalyst was denoted 40NiA with a NiO loading of 40 wt%.

For the addition of CeO_2, a modified DP method[30] was used. 0.62 g of PVPwas added to 250 mL of distilled water, followed by the addition of 0.50 g of 40NiA powders, and the resulted mixture was thoroughly dispersed by ultrasonic treatment for 1 h. The obtained slurry was slowly heated to 80 ^oC in a water-bath under vigorous stirring. Subsequently, 0.005 M $Ce(NO_3)_3$ aqueous solution was added at a rate of 0.5 mL min^{-1}, and 0.1 M NH_4OH solution was concurrently added to control the pH value at around 8.0. The slurry was further aged for 6 h under slow stirring and cooled down to room temperature. The product was collected by centrifugation, washed twice with distilled water and ethanol, and dried at 40 ^oC in air, and finally calcined at 400 ^oC for 2 h with a heating rate

of 1 ^{o}C min^{-1}. The obtained samples were denoted hereafter as 40NiAxC (x = 3, 5 and 7), where x represented the mass percent of CeO_2 deposition. It should be pointed out that the real Ni loadings of 40NiAxC were slightly lower than 40 wt% due to the addition of CeO_2 to 40NiA.

The catalysts with the same composition of 40NiA5C were also prepared by CI and SI methods respectively. For CI method, the aqueous solutions of stoichiometric quantities of $Ce(NO_3)_3 \cdot 6H_2O$ and $Ni(NO_3)_2 \cdot 6H_2O$ were mixed together. After addition of the γ-Al_2O_3 support, the suspension was stirred overnight, and then evaporated at 80 ^{o}C to remove water. The sample was dried in air at 100 ^{o}C for 24 h, and calcined at 400 ^{o}C for 2 h in air with the heating rate of 1 ^{o}C min^{-1}. The catalyst was denoted as 40NiA5C-CI. For SI method, 40NiA was impregnated with the solution of cerium nitrate followed by drying and calcining under the same conditions, and the catalyst was denoted as 40NiA5C-SI.

The catalysts with 20 wt% NiO loading were also prepared with the same methods mentioned above, and the detailed experimental procedures, characterization and catalytic tests data were described in the supporting information. In addition, a commercial Ni/Al_2O_3 catalyst HT-1 (57 wt% NiO loading) was purchased from Liaoning Haitai Sci-Tech Development Co., Ltd., China. CeO_2 powder used in this paper was made by precipitation method. The procedure was same as that of 40NiAxC only without addition of 40NiA and PVP, and the product was calcined at 400 ^{o}C for 2 h in air with the heating rate of 2 ^{o}C min^{-1}.

2.2. Catalysts characterization

X-ray diffraction (XRD) patterns were recorded on a PANalytical X'Pert PRO MPD with a step of 0.02^{o} using the Cu Kα radiation (λ=1.5418 Å) at 40 KV and 40 mA, and checked with the card number of Joint Committee on Powder Diffraction Standards (JCPDS). The crystal size of the

sample was calculated using the Debye-Scherrer equation. N_2 adsorption at −196 ^oC was measured using a Quantachrome surface area & pore size analyzer NOVA 3200e. Prior to the measurement, the sample was degassed at 200 ºC for 4 h under vacuum. The specific surface area was determined according to the Brunauer-Emmett-Teller (BET) method in the relative pressure range of 0.05−0.2. The pore size distribution (PSD) was calculated with the Barett-Joyner-Halenda (BJH) method using the adsorption isotherm branch. The microscopic feature of the samples was observed by field emission scanning electron microscope (SEM) (JSM-6700F, JEOL, Tokyo, Japan) and transmission electron microscopy (TEM) (JEM-2010F, JEOL, Tokyo, Japan). Before the TEM measurement, the H_2-reduced catalysts were cooled to room temperature in H_2 flow and then passivated in 1 vol% O_2/Ar gas mixture for 30 min to prevent bulk oxidation of the Ni NPs. Thermogravimetric (TG) analysis was conducted on a Seiko Instruments EXSTAR TG/DTA 6300. 10 mg of the sample was used and heated under air (200 mL min^{-1}) from room temperature up to 1000 ^oC (10 ^oC min^{-1}). Zeta potential analysis was carried out on a Beckman Coulter DelsaNano C particle size and zeta potential analyzer. The powders (40NiA, γ-Al_2O_3 and NiO) were mixed with 250 mL distilled water and 0.6253 g PVP, and the mixture was treated by ultrasonic for 1 h. $Ce(OH)_3$ used in zeta potential analysis was made by the method similar to that for 40NiAxC catalysts only without addition of 40NiA during the process. The pH values were adjusted by the addition of 0.1 M HCl or NaOH aqueous solution. H_2 temperature-programmed reduction (H_2-TPR) and H_2 temperature-programmed desorption (H_2-TPD) were carried out on Quantachrome Automated chemisorption analyzer (chemBET pulsar TPR/TPD). For H_2-TPR, 0.05 g sample was loaded in a quartz U-tube and heated from room temperature to 200 ^oC at 10 ^oC min^{-1} and maintain for 1 h under Ar flow. Then, the sample was cooled to room temperature and followed by heating to 1000 ^oC at 10 ^oC min^{-1} under a binary gas (10 vol % H_2/Ar) with a gas flow of 30 mL·min^{-1}. For H_2-TPD,

0.2 g catalyst was used and reduced in situ by H_2/Ar flow previously. Then, the sample was cooled to room temperature and saturated with H_2. After removing the physically adsorbed H_2 by flush with Ar for 2 h, the sample was heated to 850 ^oC ramping at 10 ^oC min^{-1} in Ar flow (30 mL min^{-1}). The consumed or desorbed H_2 was detected continuously as a function of increasing temperature using a thermal conductivity detector (TCD). The number of surface Ni sites per unit mass of catalyst was determined by means of H_2-TPD assuming the adsorption stoichiometry of H/Ni=1:1. The peak area of H_2-TPD profile was normalized by that of H_2-TPR of a standard CuO sample. The dispersion of Ni was calculated based on the volume of chemisorbed H_2 using the following simplified equation:

$$D(\%) = \frac{2 \times V_{ad} \times M \times SF}{m \times P \times V_m \times d_r} \times 100$$

where V_{ad} (mL) represented the volume of chemisorbed H_2 at the standard temperature and pressure (STP) conditions measured in the TPD procedure; m was the sample weight (g); M was the molecular weight of Ni (58.69 g mol^{-1}); P was the weight fraction of Ni in the sample as determined by ICP; SF was the stoichiometric factor (the Ni:H molar ratio in the chemisorption) which was taken as 1 and V_m was molar volume of H_2 (22414 mL mol^{-1}) at STP; d_r was the reduction degree of nickel calculated based on H_2-TPR.

2.3. Catalytic Measurement

The CO methanation reaction was carried out in a fixed bed reactor equipped with a quartz tube at 0.1 MPa and a stainless steel tube at 3.0 MPa respectively.[20] The influence of mass transfer had been examined and eliminated before the catalytic tests. First, 0.05 g catalyst sample (20−40 mesh) diluted with 5.0 g (2.5 g at 3.0 MPa) quartz sands (20−40 mesh) was uploaded in quartz tube with

an inner diameter of 8 mm. The addition of the quartz sands was to avoid the generation of hotspot in the catalyst bed. For test at 3.0 MPa, the above quartz tube was then packed in the stainless steel tube. A thermocouple was inserted into the furnace chamber and bonded to the outside of the reactor tube near the middle position of the catalyst bed to control the reaction temperature. The catalysts were reduced at 600 ^{o}C in pure H_2 (100 mL min^{-1}) for 2 h and then cooled to the starting reaction temperature in H_2. The mixed H_2 and CO as well as N_2 (as an internal standard) were introduced into the reactor at a molar ratio of H_2/CO/N_2=3/1/1 and a total flow rate of 200 mL min^{-1} with the WHSV of 240000 mL g^{-1} h^{-1}. The outlet gas stream from the reactor was cooled using a cold trap. Inlet and outlet gases were analyzed on line by Micro GC 3000A (Agilent Technologies) after 1 h (0.1 MPa) or 2.4 h (3.0 MPa) of steady-state operation at each temperature. The concentrations of H_2, N_2, CH_4, and CO in gas products were detected by a TCD detector with a Molecular Sieve column while the concentrations of CO_2, C_2H_4, C_2H_6, C_3H_6, and C_3H_8 were analyzed by another TCD with a Plot Q column. Stability test at 3.0 MPa was carried out using the fresh catalyst. After being reduced in pure H_2 at 600 ^{o}C for 2 h, the catalysts were cooled to reaction temperature and the H_2 flow was changed to reaction mixture gas to perform the stability test. Here, we defined:

$$\text{CO conversion:}\quad X_{CO}(\%) = \frac{V_{CO,in} - V_{CO,out}}{V_{CO,in}} \times 100$$

$$\text{CH}_4\text{ selectivity:}\quad S_{CH_4}(\%) = \frac{V_{CH_4,out}}{V_{CO,in} - V_{CO,out}} \times 100$$

$$\text{CH}_4\text{ yield:}\quad Y_{CH_4}(\%) = \frac{X_{CO} \times S_{CH_4}}{100} = \frac{V_{CH_4,out}}{V_{CO,in}} \times 100$$

Where $V_{i,\,in}$ and $V_{i,\,out}$ were the volume flow rate of species i (i=CO or CH_4) at inlet and outlet respectively. Blank test was carried out with 5.0 g quartz sands and the maximum of CO conversion was less than 2% under our experimental condition.

3. Results and discussion

3.1. Characterization of the catalysts

Fig. 1 shows the N_2 adsorption-desorption isotherms and PSD curves of the γ-Al_2O_3 support and the catalysts. The adsorption-desorption isotherm profiles of all the samples are all compliance with the type IV features of mesoporous materials (Fig. 1a). The PSD curves of the catalysts loaded with NiO and CeO_2 are slightly different from that of γ-Al_2O_3 support, as the former curves have small ratio of pore size at 6−8 nm (Fig. 1b), indicating that some nanoparticles (NPs) may enter the pores of γ-Al_2O_3. Furthermore, the PSD curves of the 40NiAxC and 40NiA catalysts are similar, while those of 40NiA5C-CI and 40NiA5C-SI are different, suggesting variation of CeO_2 distributions in the catalysts synthesized by different methods. Table 1 compiles the surface areas and pore volumes of the support and catalysts. The porous γ-Al_2O_3 support has a surface area of 300 m^2 g^{-1}, which is decreased to 206 m^2 g^{-1} (40NiA) after loaded with NiO, probably because the pores are blocked by NiO NPs. However, the surface areas and total pore volumes of 40NiAxC become larger compared with that of 40NiA, probably due to the fact that some CeO_2 NPs are not inserted into the pores but located on the outer surface of 40NiA catalyst. In contrast, the 40NiA5C-CI and 40NiA5C-SI catalysts have lower surface areas than that of 40NiA, because some of the pores may be blocked by CeO_2 NPs and the density of CeO_2 is larger than that of Al_2O_3.

Fig. 2A shows the XRD patterns of the reduced catalysts and CeO_2. For 40NiA, the peaks at 37.44, 44.37, and 67.25^o are attribute to the characteristic diffraction peaks of γ-Al_2O_3 (JCPDS 00-034-0493), while those at 44.64, 51.81 and 76.59^o correspond to the (111), (200) and (220) diffractions of metallic Ni (JCPDS 01-070-1849). After addition of CeO_2, a new peak at about 28.02^o appears in the XRD pattern of 40NiAxC catalysts, which corresponds to (111) diffraction of

CeO_2 (JCPDS 01-089-8436). The peak intensities of CeO_2 for all the catalysts are very weak and difficult to be discerned in some cases, indicating the high dispersion degree of CeO_2 over the catalyst surfaces. In addition, the peak intensities of Ni over these catalysts are different, and the calculated Ni particle sizes are listed in Table 1. It can be seen that the Ni particle sizes of 40NiAxC and 40NiA5C-SI are a little smaller than that of 40NiA, probably due to the presence of CeO_2 in the former catalysts that can physically separate the Ni particles from each other. This steric hindrance by CeO_2 can help these Ni particles maintain their original shape and size during the H_2 reduction process at high temperature. In contrast, the Ni particle size on 40NiA5C-CI is bigger than that of 40NiA, implying that the Ni particles are worse dispersed and the addition of CeO_2 does not facilitate the dispersion of Ni probably because of the competitive adsorption of Ni^{2+} and Ce^{3+} occurring during the CI process.

Fig. 2B presents the H_2-TPR profiles of CeO_2 and the catalysts. There is a weak peak at 447 ^oC in the H_2-TPR profile of CeO_2, corresponding to the reduction of Ce^{4+} to Ce^{3+}.[31] Because of the small amount of CeO_2 in the catalysts and the weak intensity of its reduction peak, we will focus on the reduction behaviors of NiO. The reducible NiO species in the catalysts can be approximately classified into three types: α-type (weak interaction of the NiO with support, 290−475 ^oC), β-type (mid-interaction, 475−753 ^oC), and γ-type (strong interaction, 753−894 ^oC).[20, 27] In the H_2-TPR curves of 40NiA, 40NiA5C-CI and 40NiA5C-SI prepared by different impregnation methods, there are all two major peaks, but there is only one broad peak in the curves of 40NiAxC catalysts. For 40NiA5C-CI, the two peaks belong to the reduction of α-type NiO, indicating a weak interaction of NiO with the support, as evidenced by the big Ni particle size in this sample (Table 1). For 40NiA and 40NiA5C-SI, the peaks at the low temperature belong to α-type, while those at high temperature are diffusing in a wide range, attributing to the reduction of highly-dispersed NiO

species with a strong bonding to the Al_2O_3 support. Moreover, it should be noted that the intensity ratio between the low-temperature and the high-temperature peaks of 40NiA5C-SI is smaller than that of 40NiA, indicating a stronger interaction between NiO and the support over 40NiA5C-SI. As a result, smaller Ni particle size in 40NiA5C-SI is observed than that in 40NiA (Table 1). For 40NiAxC, the H_2 consumption peak below 370 ^oC is disappeared, while the intensity of the peak above 370 ^oC is increased obviously compared with the curve of 40NiA. This may be because the NiO (especially the free NiO) in 40NiA is covered by CeO_2 after the addition of CeO_2, thus the NiO species become more difficult to be reduced with the shift of the H_2 consumption peak below 370 ^oC to high temperature.

Fig. 2C shows the H_2-TPD profiles of CeO_2 and catalysts, and Table 1 lists the calculated hydrogen uptake values and Ni dispersion of the catalysts based on the H_2-TPR and H_2-TPD results. For CeO_2, it has a strong H_2 desorption peak at 415 ^oC, suggesting CeO_2 can increase the hydrogen uptake of the catalyst, which is accordant with the literature results.[32, 33] It can be seen that the H_2-TPD profiles of all the catalysts are similar and exhibit three H_2 desorption peaks around 218, 357 and 699 ^oC respectively, while there is no obvious desorption peak at about 415 ^oC, indicating the H_2 absorption of CeO_2 on the catalysts is negligible. In addition, γ-Al_2O_3 used in this work is stable and the weight loss is only 2.6 wt% at 1000 ^oC detected by TG in air (not shown here). The intensity of H_2-TPD profile of γ-Al_2O_3 (not shown here) is very weak compared with that of the catalysts. Thus, the effect of the support Al_2O_3 can be neglected. The first peak at low temperature (218 ^oC) can be attributed to chemisorbed hydrogen on the highly dispersed Ni NPs with a large density of surface defects, which can serve as capture traps for surface hydrogen diffusion so as to reduce the activation energy of hydrogen dissociation.[30] The second peak (357 ^oC) is attributed to hydrogen adsorbed at bulk or lowly-dispersed Ni NPs. In addition, the peak located at around 669

°C can be attributed to the H_2 adsorbed in the subsurface layers of Ni atoms and/or to the spillover H_2.[34] For 40NiAxC, there is an obvious increase in the integral area of the H_2 uptake peaks comparing with that of 40NiA, indicating more Ni sites are exposed to H_2. Meanwhile, there is an increase in the amount of surface-dissociated H_2 or spillover H_2 due to the contribution of CeO_2. Table 1 reveals that the addition of proper amount of CeO_2 can increase the H_2 uptake and the dispersion of Ni in the 40NiAxC catalysts, and 40NiA5C has the highest total H_2 uptake of 378.5 μmol g_{cat}^{-1} and Ni dispersion of 14.9%. However, excess CeO_2 may cover some of the surface Ni atoms, thus the H_2 uptake and Ni dispersion of 40NiA7C are decreased again compared to those of 40NiA5C. 40NiA5C-SI also has a high H_2 uptake of 330.7 μmol·g_{cat}^{-1} and a Ni dispersion of 13.0%, close to that for 40NiA5C. Although 40NiA5C-CI has the same composition as 40NiA5C and 40NiA5C-SI, its H_2 uptake is much lower due to its bigger Ni particle size.

The Nitrogen adsorption, XRD, H_2-TPR and H_2-TPD tests over the catalysts with 20 wt% NiO are also conducted, and similar trends to those over the catalysts with 40 wt% NiO are observed (Fig. S1−2 and Table S1−2).

Fig. 3 shows the TEM images of the reduced 40NiAxC catalysts. No obvious Ni particles agglomerations in the reduced 40NiAxC catalysts is observed, and the Ni particle sizes are about 5−35, 5−15 and 5−25 nm in 40NiA3C (Fig. 3a), 40NiA5C (Fig. 3b) and 40NiA7C (Fig. 3c), respectively. CeO_2 nanocrystallites cannot be identified in the TEM images due to the poor contrast between Al_2O_3 and CeO_2. Fig. 3d shows the HRTEM images of 40NiA7C. The observed lattice spacing of ca. 0.20 nm corresponds to the Ni (111) plane, as reported previously,[27] which is closely related to the active sites for the methanation reaction. The lattice spacing at ca. 0.31 nm corresponds to the CeO_2 (111) plane and the CeO_2 nanocrystallites are well dispersed among or closely connect with the Ni particles.

3.2. Catalytic properties of the catalysts

CO methanation was first carried out in the temperature range of 300−600 ^{o}C at 0.1 MPa and a WHSV of 240000 mL g^{-1} h^{-1}, and the results are listed in Fig. 4a−c. Overall, the CO conversion and CH_4 yield of all the catalysts present volcano-shaped trends with increase of the reaction temperature. This is because CO methanation is a strongly exothermic reaction and the high temperature has adverse effect on this reaction.[5] After addition of CeO_2, the activities of 40NiAxC catalysts are improved significantly compared with those of 40NiA. After addition of CeO_2, the activities of 40NiAxC catalysts are improved significantly compared with those of 40NiA, and the maximum of CO conversion and CH_4 yield are obtained over 40NiA5C with 99 and 85% respectively at 350 ^{o}C. For 40NiA7C, although it has more CeO_2, its activity becomes lower, probably due to the coverage of active sites by CeO_2. The CO conversion and CH_4 yield of 40NiA5C-SI are also lower than those of 40NiA5C, although its CH_4 selectivity of 40NiA5C-SI is close to that of 40NiA5C. Meanwhile, the activity of 40NiA5C-CI is much lower than that of the others. In addition, compared to 40NiA, the low-temperature CO methanation below 350 ^{o}C over the catalysts with the addition of CeO_2 are all enhanced except for 40NiA5C-CI at 300 ^{o}C. For 40NiA5C, the CO conversion is 84% and the CH_4 yield is 68% at 300 ^{o}C, which is higher than the maximum value of the CO conversion and CH_4 yield over 40NiA at 450 ^{o}C. In short, the addition of CeO_2 on Ni/Al_2O_3 can enhance the CO methanation obviously at atmospheric pressure. In addition, thermodynamic equilibrium analysis of CO methanation at different conditions was systematically carried out previously.[29] CO conversion on 40NiA5C nearly reaches the equilibrium at 350−450 ^{o}C, but lower than equilibrium below 350 ^{o}C and beyond 450 ^{o}C. On the contrast, CO conversion on others catalysts is under the equilibrium in the total temperature range. On the other hand, the CH_4 selectivity on all the catalysts can reach equilibrium only at 450 ^{o}C, while it is lower below 450 ^{o}C

but higher than equilibrium above 450 °C. Xavier *et al.*,[15] also reported the doping of CeO_2 on Ni/Al_2O_3 could improve the activity of the catalyst for CO methanation. They found Ce^{3+} sites had strong interactions with oxygen atom of the chemisorbed CO molecules, which weakened the CO bond and thus facilitated the formation of surface carbon. The later was further hydrogenated to form methane. It should be pointed out that the activity sequence of all the catalysts is accordant with that of H_2 uptake and Ni dispersion shown in Table 1. Moreover, similar trends are also observed over the catalysts with 20 wt% NiO, and the best catalyst is 20NiA3C (Fig. S3).

CO methanation over the best catalyst of 40NiA5C is also carried out at 3.0 MPa and a WHSV of 240000 mL g^{-1} h^{-1} because this reaction is a volume-reduced and normally conducted at high pressure (2.94−3.43 MPa) in industry.[35] For comparison, 40NiA and a high NiO loading commercial methanation catalyst HT-1 are also tested, and the results are shown in Fig. 4d−f. The CO conversion over these three catalysts is very close to thermodynamics equilibrium[29], and it can reach 100% at 300−450 °C, then a decrease occurs at higher temperature for exothermic character of CO methanation (Fig. 4d). At the same time, 40NiA5C has the highest CH_4 selectivity and CH_4 yield (except for 600 °C) among the above catalysts. Obviously, 40NiA5C is a competitive catalyst, even to the commercial methanation catalyst HT-1 (Fig. 4e−f).

The life time test is essential for evaluation of a catalyst, and maintaining the activity and stability of the catalyst under harsh reaction conditions is crucial for the industrial process. However, some literature works only evaluated their catalysts at low temperature and low WHSVs under atmospheric or low pressures,[9, 10] although their activities were reported to be stable more than 100 h. Therefore, these data for evaluation of thermal stability and resistance to carbon deposition of the catalysts are not sufficient. In order to study the coke and sintering resistance of the catalysts, we thus conduct a life time test at 300−600 °C, 3.0 MPa and a high WHSV of 240000 mL g^{-1} h^{-1}, and

the results are shown in Fig. 5. For 40NiA5C, the activity can remain constant during every time period from 300 to 600 ^{o}C, suggesting its good stability at both low and high temperature at a high WHSV. In contrast, the activity of the HT-1 catalyst can remain steady at low temperature (300 and 400 ^{o}C), but the test has to be terminated after 26 h (6 h at 500 ^{o}C) because the large pressure drop of the catalyst bed occurs (Fig. 5d). For 40NiA, the test was terminated after 31 h (1 h at 600 ^{o}C) for the same reason as HT-1, which is consistent with the previous results.[36] In Fig. 5d, the pressure drop of 40NiA5C remains constant at 0.02 MPa (the system pressure drop of the catalyst bed) during the test, indicating no obvious carbon deposition. On the contrary, the pressure drops of HT-1 and 40NiA increase quickly after 26 and 31 h respectively, suggesting serious carbon deposition occurred on them. It should be noted that the syngas methanation often runs at the high concentration of CO (with a H_2/CO feed ratio of about 3.0) and high temperature (300−600 ^{o}C),[5] which is quite different from the selective CO methanation reaction for the removal of trace CO (usually ca. 1 vol%) from the H_2 rich stream at low temperature (200−250 ^{o}C).[37] Thus, HT-1 may be a commercial selective CO methanation catalyst with a high loaded NiO (57 wt%). Additionally, a life time test of 40NiA5C is also carried out at 600 ^{o}C, 3.0 MPa and a WHSV of 30000 mL g^{-1} h^{-1}, and the catalytic activity of this catalyst can also remain constant for 104 h which further testifies its good thermal stability at high temperature (Fig. S4). Furthermore, 40NiA5C and 40NiA are also molded by a tablet press machine, which are denoted 40NiA5C-G and 40NiA-G respectively (Fig. S5). The crushing strengths of the three catalysts are also tested. The radial and axial crushing strengths of 40NiA5C-G and 40NiA-G are a little higher or comparable compared with those of HT-1 (Table S3). The catalytic performance of the three catalysts is also tested at 3.0 MPa and a WHSV of 30000 mL g^{-1} h^{-1}. It can be seen that the activities of 40NiA5C-G and 40NiA-G are close to those of HT-1, especially, the CH_4 yield of 40NiA5C-G can be higher than that of HT-1 in the

temperature range of 300−550 °C (Fig. S6), indicating the activity of 40NiA5C can be very high both before and after molding.

3.3. Characterization of the spent catalysts

Fig. 6a shows the XRD patterns of the used HT-1, 40NiA5C and 40NiA catalysts after life time test as well as the freshly reduced HT-1. The Ni particle size of the used 40NiA5C is calculated to be 9.3 nm, a little larger than that of the freshly reduced 40NiA5C (8.3 nm), indicating the good thermal stability of 40NiA5C. In contrast, the Ni particle sizes of HT-1 and 40NiA increase from 9.9 to 17.9 nm and from 9.5 to 13.6 nm after the life time test respectively, suggesting their poor thermal stabilities at high temperatures. On the other hand, there is a new diffraction peak at 26.55° in the XRD patterns of the used HT-1 and 40NiA, corresponding to graphitic carbon (JCPDS 03-065-6212). It is known that the deposited carbon may have various forms such as amorphous carbon, vermicular carbon and graphitic carbon,[38] but only graphitic carbon can be detected apparently by XRD. The carbon peak in the XRD pattern is very weak, indicating the graphitic carbon is not well crystallized in the used HT-1 and 40NiA. Of course, the formation of amorphous carbon still cannot be excluded. The amount of the deposited carbon on the used catalysts is determined by TG analysis, as presented in Fig. 6b. The carbon content in the used HT-1 and 40NiA catalyst is estimated to be 10.0 and 4.0 wt % respectively, while it is only 0.8 wt % for the used 40NiA5C catalyst. From the SEM images it can be seen that there are many filamentous carbons formed on the surface of the used HT-1 (Fig. 6c), and some filamentous carbons can be also found over 40NiA catalyst (Fig.6e), however, filamentous carbon is absent in the used 40NiA5C (Fig. 6d). There are two questions perplexing us, one is that the carbon amounts of the used HT-1 and 40NiA are still not very high, contradictory to the fact that the catalyst beds were blocked during the life time test; the second is that although there is 0.8 wt% carbon on the used

40NiA5C, there is no filamentous carbon observed by SEM.

For the first question, we examine the changes of quartz tube before and after the life time test of 40NiA, and have obtained some probable causes (Fig. S7−9). Similar to the literature result,[39] the clog of the tube is mainly found on the top of the catalyst bed (Fig. S7d). As we all know the rate at which deactivation occurs for a given catalyst and reaction depends greatly on reaction conditions, especially temperature. Rates of carbon precursor formation and gasification both increase exponentially with temperature, although the difference between them varies a great deal with temperature because of differences in pre-exponential factors and activation energies.[40] Thus, once the carbon deposition is initiated, the rates of carbon formation are sufficiently high to cause catastrophic pore plugging and catalyst failure within a few hours to days. In this work, the gas stream flows through the bed from the top to bottom with high concentrations of CO and H_2 at the upper of the catalyst bed, and the larger the WHSVs the bigger the concentration difference. Hence, although some quartz sands have been added to transfer heat, the hotspots may occur at the top of the catalyst bed for the strongly exothermic CO methanation, resulting in the clog of the quartz tube. Furthermore, from the results of the blank tube tests (Fig. S9) we know some deposited carbon in the catalyst bed can be eliminated by the steam produced by CO methanation, while there is no steam at the top of the catalyst bed, which may be the main reason for that the clog of quartz tube found on the top of the catalyst bed rather than the upper. On the other hand, Ni particle size will also affect the growth rate of carbon filaments on the catalysts. Chen *et al.,*[41] has reported that the optimum growth rate and yield of carbon nanofibers could be achieved on optimally sized Ni crystals (around 34 nm), and small Ni crystals yielded a low growth rate. The Ni particle size of the used 40NiA that is recycled from the top of the catalyst bed is 18.4 nm (Fig. S8d), so it will also enhance the growth of the carbon filaments. Therefore, carbon deposition and sintering occur

simultaneously and reinforce each other at high temperature, which cause the termination of HT-1 and 40NiA life time test in the short time.

For the second question, CeO_2 has been reported to have positive effect on carbon suppression when used as a promoter in Ni/Al_2O_3 catalysts for steam reforming,[42, 43] as CeO_2 could increase supply of active oxygen species on the Ni surface due to enhanced water adsorption and gasification. In this work, since there is no graphitic carbon detected by both XRD and SEM in the used 40NiA5C, and the carbon content measured by TG is 0.8 wt%, the deposited carbon on 40NiA5C is likely to be amorphous carbon. Recently Lu *et al.,*[44] has found that the $CeAlO_3$ of $Ni/CeAlO_3$-Al_2O_3 catalyst could inhibit the growth of filamentous carbon on Ni surface while the formation of amorphous carbon via thermal cracking of methane is independent of $CeAlO_3$. Hence, the CeO_2 in the 40NiA5C may play a similar role, which mainly inhibit growth of graphitic carbon but not workable to the growth of the amorphous carbon.

Furthermore, as mentioned that the Ni particle size of the reduced and used 40NiA5C is 8.3 and 9.3 nm respectively, it indicates good sintering resistance of 40NiA5C. An effective approach to control sintering proposed in the literature was the addition of a second component or an oxide phase that is applied as an overcoat.[45] In this work, CeO_2 is deposited on the surface of 40NiA which may play a similar function like the overcoat; CeO_2 can be physical barrier for Ni particles, which restrains the increase of Ni particle size during the process of reduction and reaction conditions at high temperature.

From the above results, it can be seen 40NiA5C catalyst has the highest activity for CO methanation as well as the best resistance to carbon deposition and Ni NPs sintering. A proposed reaction process and outline for the structure-property relationship are given in Fig. 7. For 40NiA, Ni particles will agglomerate in the process of reduction at high temperature because of particle

migration or Ostwald ripening[19] (seen in Table 1) (Fig. 7a). For 40NiA 5C-SI, CeO_2 can distribute on the surface of Al_2O_3 and NiO uniformly with high dispersion, because Ce^{3+} can adsorb on the surface of 40NiA freely, and the CeO_2 particles can restrain the growth of Ni particles during the reduction at high temperatures leading to small Ni particles (Fig. 7b).

To further confirm the structure of 40NiA5C, zeta potentials analysis of 40NiA, γ-Al_2O_3, NiO and the precursor of CeO_2 ($Ce(OH)_3$) are measured. The zeta potential of PVP-stabilized 40NiA, γ-Al_2O_3 and NiO is 7.9, −9.0 and 14.4 mV respectively. NiO shows a positive zeta potential, indicating that NiO bears a positive surface charge, which is consistent with the result of Xiang *et al*.[46] In contrast, $Ce(OH)_3$ is negatively charged with a zeta potential of −13.2 mV in the turbid liquid, so it will selectively adsorb onto the surface of NiO particles due to the electrostatic attraction.[47] Therefore, CeO_2 should mainly distribute on the surface of NiO rather than on Al_2O_3 in 40NiA5C, and CeO_2 can enhance the interaction of NiO and support and act as a physical barrier to restrain growth of Ni particles resulting in small Ni particle size during the reduction. The results of aforementioned N_2 adsorption, XRD, H_2-TPR and H_2-TPD also supported this inference and the proposed formation process of 40NiA5C is illustrated in Fig. 7c. The presence of electrostatic interaction and selective deposition is the critical factor for precipitation-deposition method. The proper distribution of CeO_2 on Ni/Al_2O_3 enhances the promotion effect of CeO_2, which leads to the excellent catalytic performance and stability of 40NiA5C for CO methanation.

In the preparation process of 40NiA5C-CI, the competitive adsorption of Ni^{2+} and Ce^{3+} occurs during the co-impregnation process. Ce^{3+} ions adsorbs on Al_2O_3 preferentially with high dispersion on the support; on the contrary, the Ni^{2+} ions adsorption will be difficult for the steric hindrance and electrostatic repulsion of Ce^{3+} ions, which results in poor dispersion of Ni^{2+} ions and large Ni particle size of 40NiA5C-CI (Fig. 7d).

4. Conclusions

We report the preparation and characterization of CeO_2-decorated Ni/γ-Al_2O_3 catalysts with a NiO loading of 40 wt% for CO methanation. Compared with the Ni catalysts prepared by the CI and SI methods, the catalyst of 40NiA5C derived from DP method shows the enhanced catalytic performance, which remains high activity and very good carbon and sintering resistance in the life test. In the modified DP procedure, CeO_2 can selectively deposit on the surface of NiO rather than Al_2O_3 due to the electrostatic interaction, which on the one hand can act as a physical barrier to restrain the growth of the Ni particles during the reduction and catalytic reaction at high temperatures and thus effectively inhibit the sintering of the Ni particles, and on the other hand can reduce the coke formation by suppressing the growth of graphitic carbon via increasing active oxygen species on the Ni surface. This unique structural characteristic enhances the promotion effect of CeO_2, and achieves simultaneous inhibition of coke and sintering of Ni particles in 40NiA5C, while maintaining high catalytic activity for CO methanation.

Acknowledgments

The authors gratefully acknowledge the supports from the National Basic Research Program (No. 2014CB744306), National Key Technology R&D Program of China (No. 2010BAC66B01), and "Strategic Priority Research Program" of the Chinese Academy of Sciences (Nos. XDA07010100 and XDA07010200).).

References

1 J. Kopyscinski, T. J. Schildhauer and S. M. A. Biollaz, *Fuel*, 2010, **89**, 1763-1783.

2 R. Razzaq, C. Li and S. Zhang, *Fuel*, 2013, **113**, 287-299.

3 M. V. Twigg and J. T. Richardson, *Appl. Catal., A*, 2000, **190**, 61-72.

4 D. C. Gardner and C. H. Bartholomew, *Ind. Eng. Chem. Prod. Res. Dev.* , 1981, **20**, 80-87.

5 J. R. Rostrup-Nielsen, K. Pedersen and J. Sehested, *Appl. Catal., A*, 2007, **330**, 134-138.

6 S. Rahmani, M. Rezaei and F. Meshkani, *J. Ind. Eng. Chem.* , 2013. DOI: 10.1016/j.jiec.2013.07.017.

7 A. Zhao, W. Ying, H. Zhang, H. Ma and D. Fang, *Catal. Commun.* , 2012, **17**, 34-38.

8 S. Hwang, J. Lee, U. G. Hong, J. G. Seo, J. C. Jung, D. J. Koh, H. Lim, C. Byun and I. K. Song, *J. Ind. Eng. Chem.* , 2011, **17**, 154-157.

9 D. Hu, J. Gao, Y. Ping, L. Jia, P. Gunawan, Z. Zhong, G. Xu, F. Gu and F. Su, *Ind. Eng. Chem. Res.*, 2012, **51**, 4875-4886.

10 M. Cai, J. Wen, W. Chu, X. Cheng and Z. Li, *J. Nat. Gas Chem.* , 2011, **20**, 318-324.

11 A. Zhao, W. Ying, H. Zhang, M. Hongfang and D. Fang, *J. Nat. Gas Chem.* , 2012, **21**, 170-177.

12 A. Trovarelli, C. de Leitenburg, M. Boaro and G. Dolcetti, *Catal. Today* 1999, **50**, 353-367.

13 R. Perez-Hernandez, G. Mondragon-Galicia, A. Allende Maravilla and J. Palacios, *Phys. Chem. Chem. Phys.* , 2013, **15**, 12702-12708.

14 H. Liu, X. Zou, X. Wang, X. Lu and W. Ding, *J. Nat. Gas Chem.* , 2012, **21**, 703-707.

15 K. O. Xavier, R. Sreekala, K. K. A. Rashid, K. K. M. Yusuff and B. Sen, *Catal. Today* 1999, **49**, 17-21.

16 L. Znak, K. Stołecki and J. Zieliński, *Catal. Today* 2005, **101**, 65-71.

17 N. Wang, K. Shen, L. Huang, X. Yu, W. Qian and W. Chu, *ACS Catal.*, 2013, **3**, 1638-1651.

18 D. W. Kim, K. D. Kim, H. O. Seo, N. K. Dey, M. J. Kim, Y. D. Kim, D. C. Lim and K. H.

Lee, *Catal. Lett.* , 2011, **141**, 854-859.

19 H. Liu, C. Guan, X. Li, L. Cheng, J. Zhao, N. Xue and W. Ding, *ChemCatChem* 2013, **5**, 3904-3909.

20 C. Jia, J. Gao, J. Li, F. Gu, G. Xu, Z. Zhong and F. Su, *Catal. Sci. Technol.*, 2013, **3**, 490-499.

21 J. Zhang, Z. Xin, X. Meng and M. Tao, *Fuel*, 2013, **109**, 693-701.

22 L. Li, Y. Yao, B. Sun, Z. Fei, H. Xia, J. Zhao, W. Ji and C.-T. Au, *ChemCatChem* 2013, **12**, 3781–3787.

23 X. Liu, A. Wang, L. Li, T. Zhang, C.-Y. Mou and J.-F. Lee, *J. Catal.* , 2011, **278**, 288-296.

24 X. Li, S. S. S. Fang, J. Teo, Y. L. Foo, A. Borgna, M. Lin and Z. Zhong, *ACS Catal.*, 2012, **2**, 360-369.

25 Q. Fu, F. Yang and X. Bao, *Acc. Chem. Res.* , 2013, **46**, 1692-1701.

26 J. Gao, C. Jia, J. Li, F. Gu, G. Xu, Z. Zhong and F. Su, *Ind. Eng. Chem. Res.*, 2012, **51**, 10345-10353.

27 J. Gao, C. Jia, M. Zhang, F. Gu, G. Xu and F. Su, *Catal. Sci. Technol.*, 2013, **3**, 2009-2015.

28 J. Gao, C. Jia, M. Zhang, F. Gu, G. Xu, Z. Zhong and F. Su, *RSC Adv.*, 2013, **3**, 18156-18163.

29 J. Gao, Y. Wang, Y. Ping, D. Hu, G. Xu, F. Gu and F. Su, *RSC Adv.*, 2012, **2**, 2358-2368.

30 J. Liu, C. Li, F. Wang, S. He, H. Chen, Y. Zhao, M. Wei, D. G. Evans and X. Duan, *Catal. Sci. Technol.*, 2013, **3**, 2627-2633.

31 Z. Abbasi, M. Haghighi, E. Fatehifar and N. Rahemi, *Asia-Pac. J. Chem. Eng.* , 2012, **7**, 868-876.

32 S. Bernal, J. J. Calvino, G. A. Cifredo, J. M. Gatica, J. A. P. Omil and J. M. Pintado, *J.*

Chem. Soc., Faraday Trans., 1993, **89**, 3499-3505.

33 M. Li, Z. Wu and S. H. Overbury, *J. Catal.* , 2013, **306**, 164-176.

34 S. Velu and S. Gangwal, *Solid State Ionics* 2006, **177**, 803-811.

35 P. Mondal, G. S. Dang and M. O. Garg, *Fuel Process. Technol.* , 2011, **92**, 1395-1410.

36 K. Y. Koo, H.-S. Roh, Y. T. Seo, D. J. Seo, W. L. Yoon and S. Bin Park, *Int. J. Hydrogen Energy* 2008, **33**, 2036-2043.

37 A. Chen, T. Miyao, K. Higashiyama, H. Yamashita and M. Watanabe, *Angew. Chem. Int. Ed.* , 2010, **49**, 9895-9898.

38 C. H. Bartholomew, *Catal. Rev.*, 1982, **24**, 67-112.

39 J. Kopyscinski, T. J. Schildhauer and S. M. A. Biollaz, *Ind. Eng. Chem. Res.*, 2010, **50**, 2781-2790.

40 C. H. Bartholomew, *Appl. Catal., A*, 2001, **212**, 17-60.

41 D. Chen, K. Christensen, E. Ochoafernandez, Z. Yu, B. Totdal, N. Latorre, A. Monzon and A. Holmen, *J. Catal.* , 2005, **229**, 82-96.

42 S. Natesakhawat, R. Watson, X. Wang and U. Ozkan, *J. Catal.* , 2005, **234**, 496-508.

43 S. Wang and G. Q. Lu, *Appl. Catal., B*, 1998, **19**, 267-277.

44 W. Chen, G. Zhao, Q. Xue, L. Chen and Y. Lu, *Appl. Catal., B*, 2013, **136-137**, 260-268.

45 J. Lu, B. Fu, M. C. Kung, G. Xiao, J. W. Elam, H. H. Kung and P. C. Stair, *Science*, 2012, **335**, 1205-1208.

46 L. Xiang, X. Y. Deng and Y. Jin, *Scr. Mater.* , 2002, **47**, 219-224.

47 Y. L. Han, Y. Yang, S. Liu, J. Wu, Y. Chen, T. J. Lu and F. Xu, *Biofabrication*, 2013, **5**, 035004.

Figure Captions

Fig. 1 N_2 adsorption isotherms (a) and PSD curves (b) of unreduced catalysts (For clarity, the isotherm of 40NiA5C-CI, 40NiA7C, 40NiA5C, 40NiA3C, 40NiA and Al_2O_3 was vertically shifted for 50, 50, 110, 140, 170 and 30 cm^3 g^{-1}, respectively.)

Fig. 2 XRD patterns (A), H_2-TPR profiles (B) and H_2-TPD profiles (C): (a) CeO_2, (b) 40NiA, (c) 40NiA3C, (d) 40NiA5C, (e) 40NiA7C, (f) 40NiA5C-CI, and (g) 40NiA5C-SI.

Fig. 3 TEM images: (a) reduced 40NiA3C, (b) reduced 40NiA5C, (c and d) reduced 40NiA7C.

Fig. 4 Catalytic properties of the catalysts at 240000 mL g^{-1} h^{-1}: (a and d) CO conversion, (b and e) CH_4 selectivity, and (c and f) CH_4 yield.

Fig. 5 Life time test of HT-1, 40NiA5C and 40NiA at 3.0 MPa 240000 mL g^{-1} h^{-1}: (a) CO conversion, (b) CH_4 selectivity, (c) CH_4 yield and (d) pressure drop of the catalyst bed during the test.

Fig. 6 XRD patterns of the catalysts after life time tests (a), TG curves of the fresh and used catalysts in air (b), and SEM images of used HT-1(c), used 40NiA5C (d), and used 40NiA (e).

Fig. 7 Schematic diagram of the formation process of 40NiA (a), 40NiA5C-SI (b), 40NiA5C (c) and 40NiA5C-CI (d).

Table 1 Physical and chemical properties of the supports and catalysts.

Samples	S_{BET}[a] ($m^2\ g^{-1}$)	V[b] ($cm^3\ g^{-1}$)	Ni particle size[c] (nm)	H_2 uptake ($\mu mol\ g^{-1}$)	D[d] (%)
γ-Al_2O_3	300	0.48	–	–	–
40NiA	206	0.26	9.9	157.7	5.9
40NiA3C	219	0.35	9.2	253.7	9.8
40NiA5C	222	0.35	8.3	378.5	14.9
40NiA7C	210	0.28	8.9	325.6	13.1
40NiA5C-CI	139	0.21	19.1	151.6	6.0
40NiA5C-SI	171	0.24	8.6	330.7	13.0

[a] Surface area of the unreduced catalysts, derived from BET equation.

[b] Pore volume of the unreduced catalysts, obtained from the volume of nitrogen adsorbed at the relative pressure of 0.97.

[c] Calculated by the XRD diffraction peak (2θ=44.64°) of the reduced catalysts using the Debye-Scherrer equation.

[d] Ni dispersion, calculated based on the H_2-TPR and H_2-TPD results.

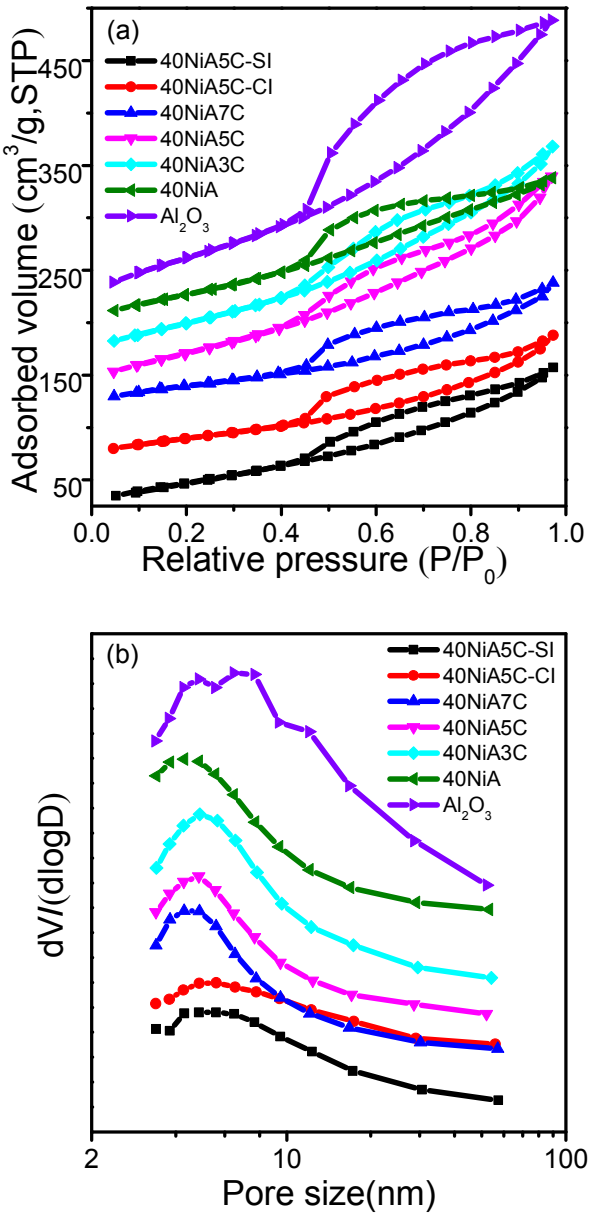

Fig. 1

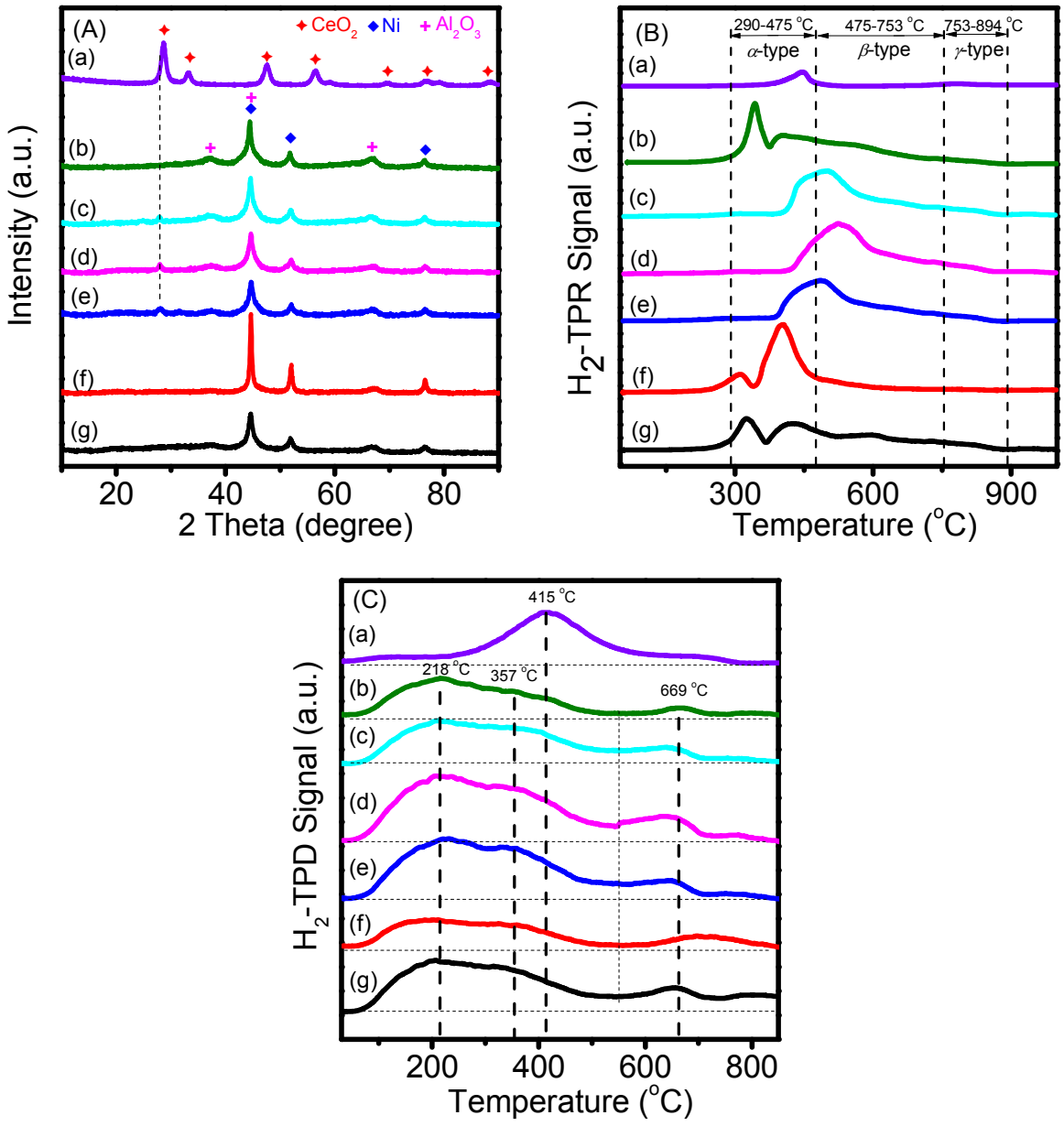

Fig. 2

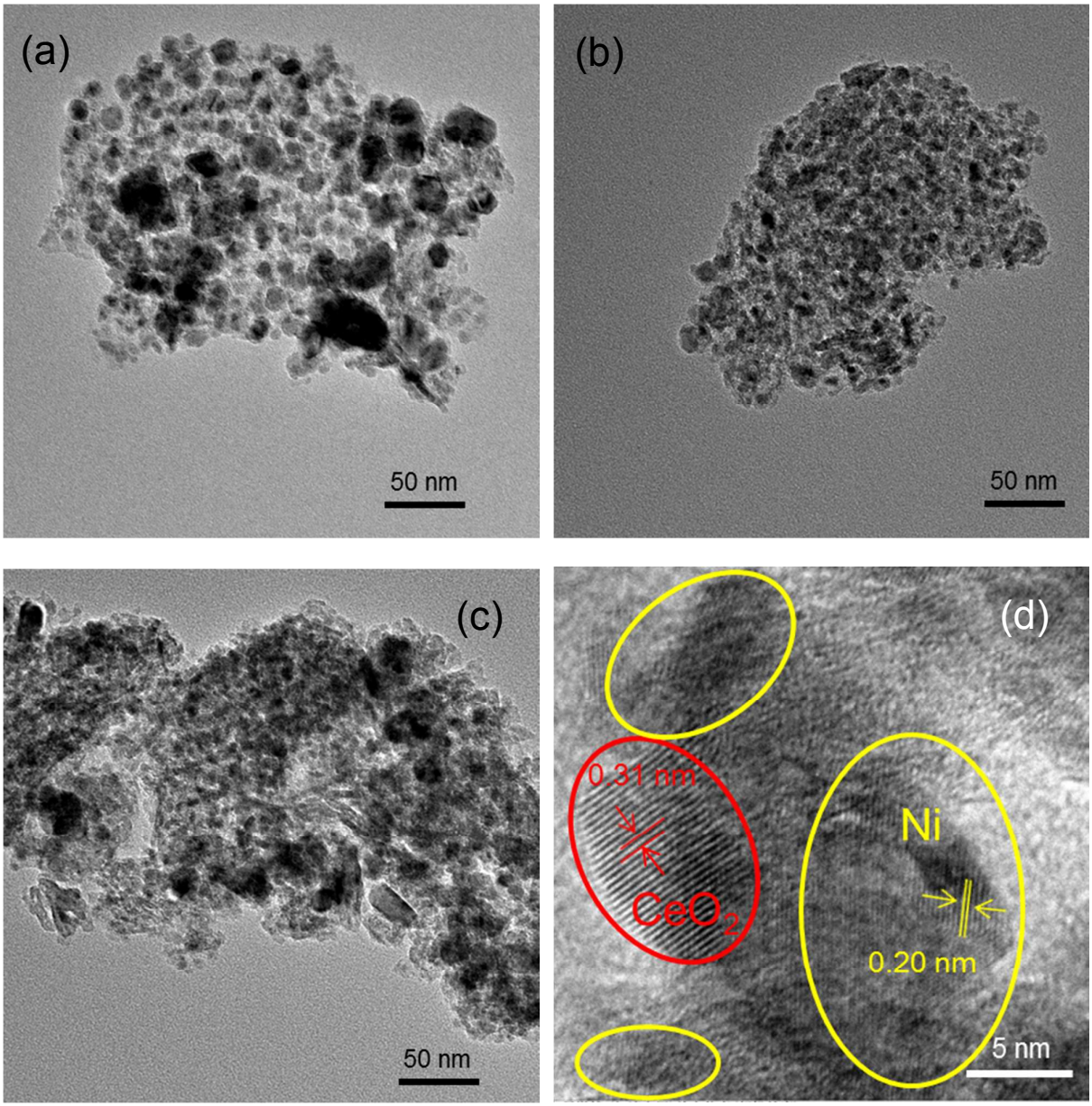

Fig. 3

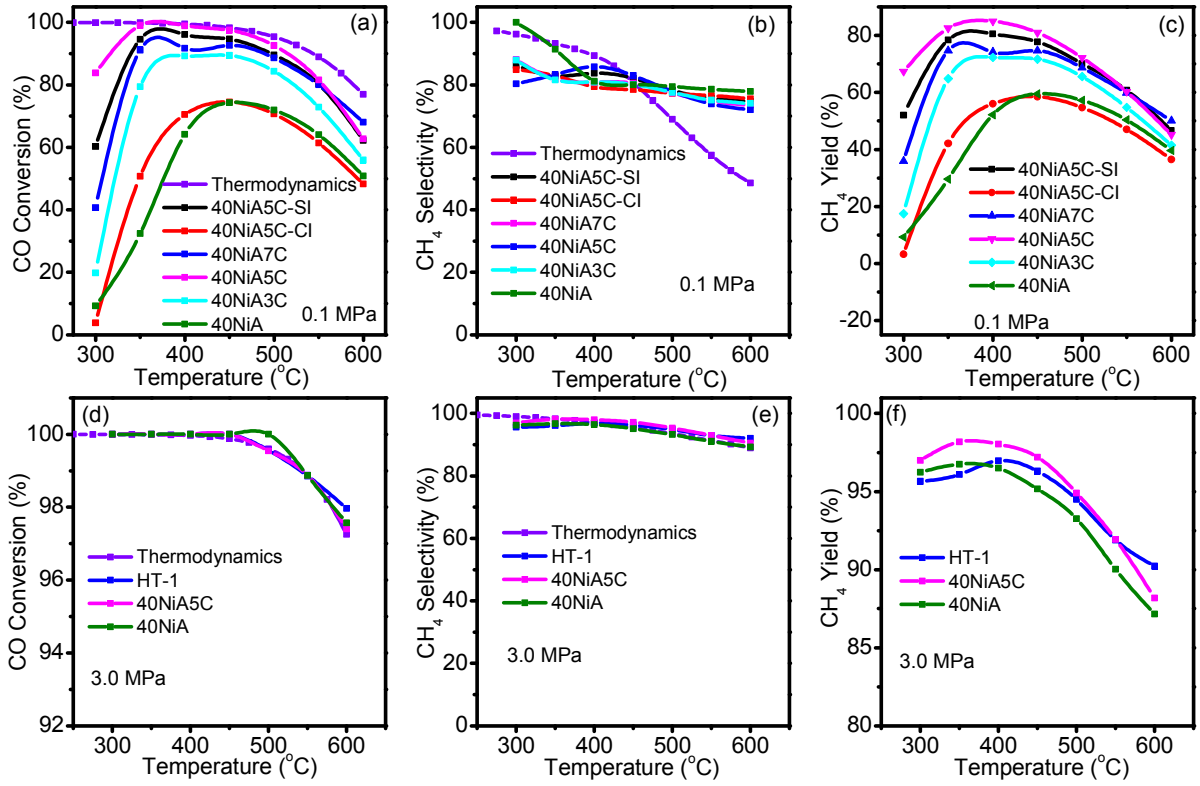

Fig. 4

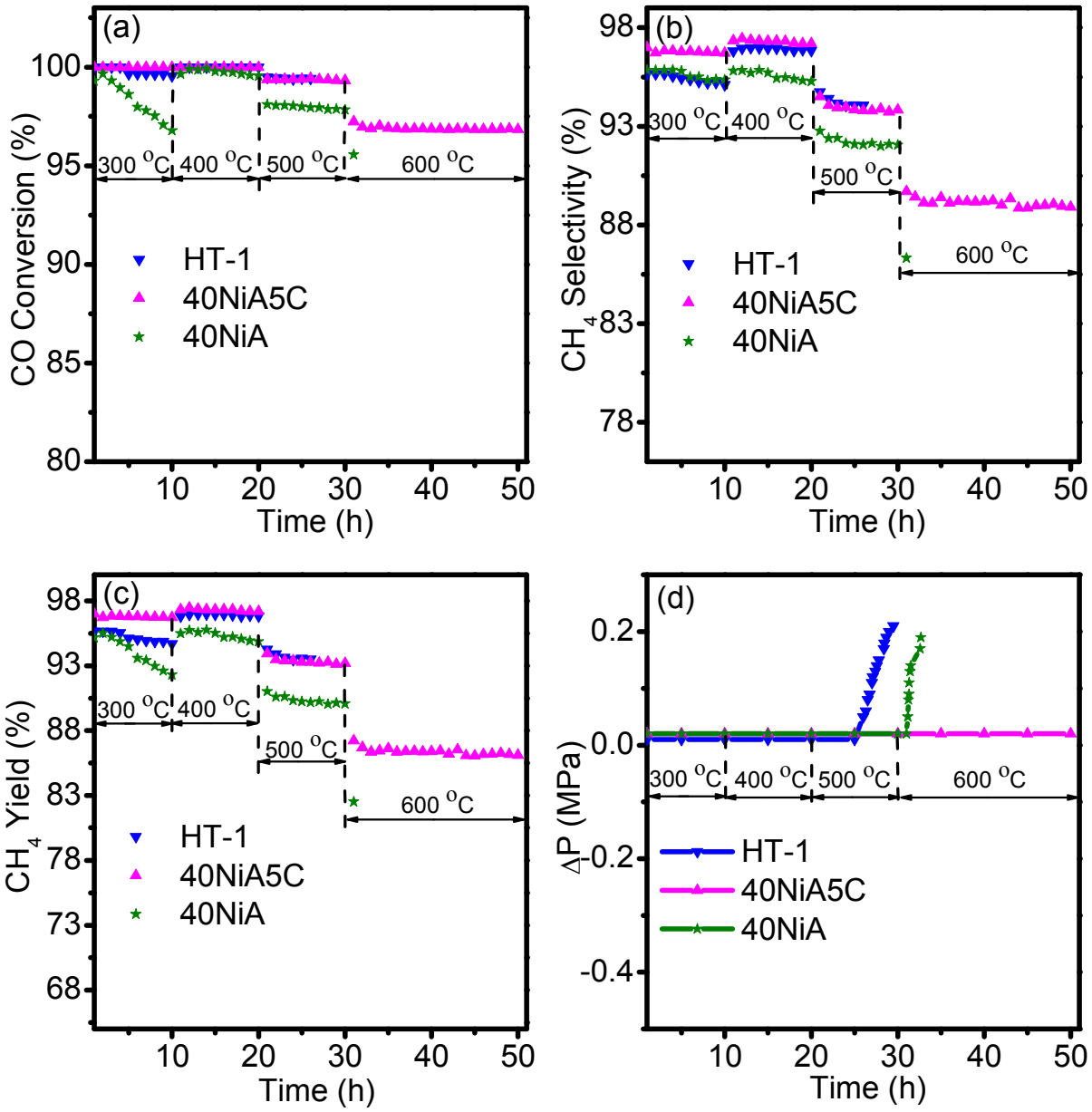

Fig. 5

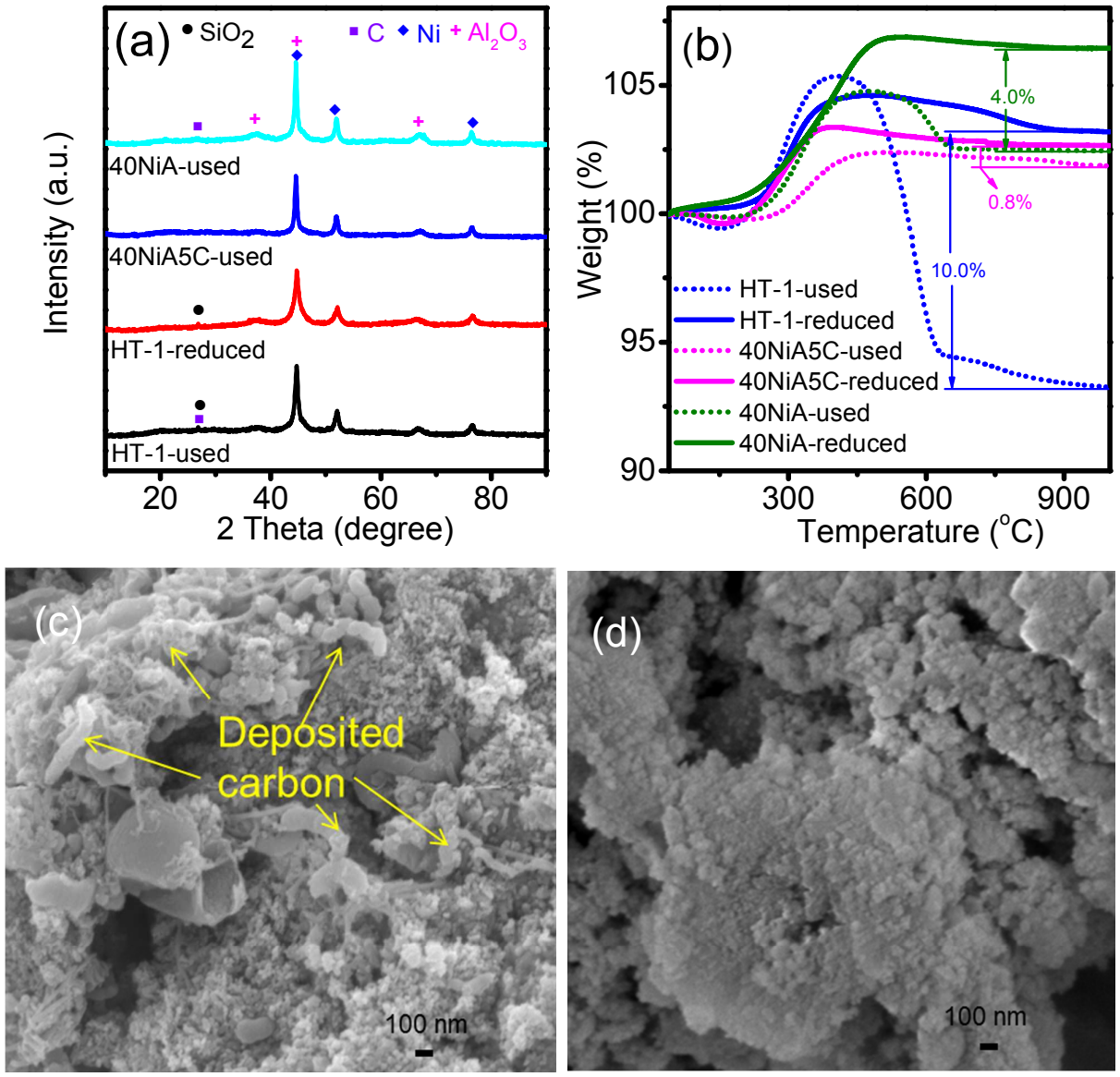

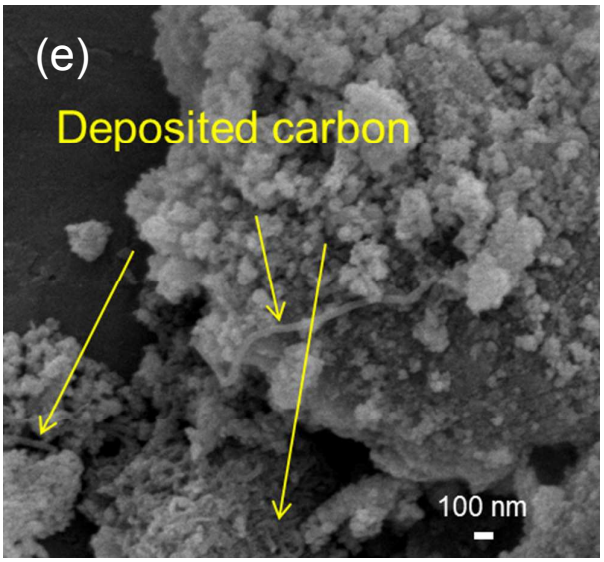

Fig. 6

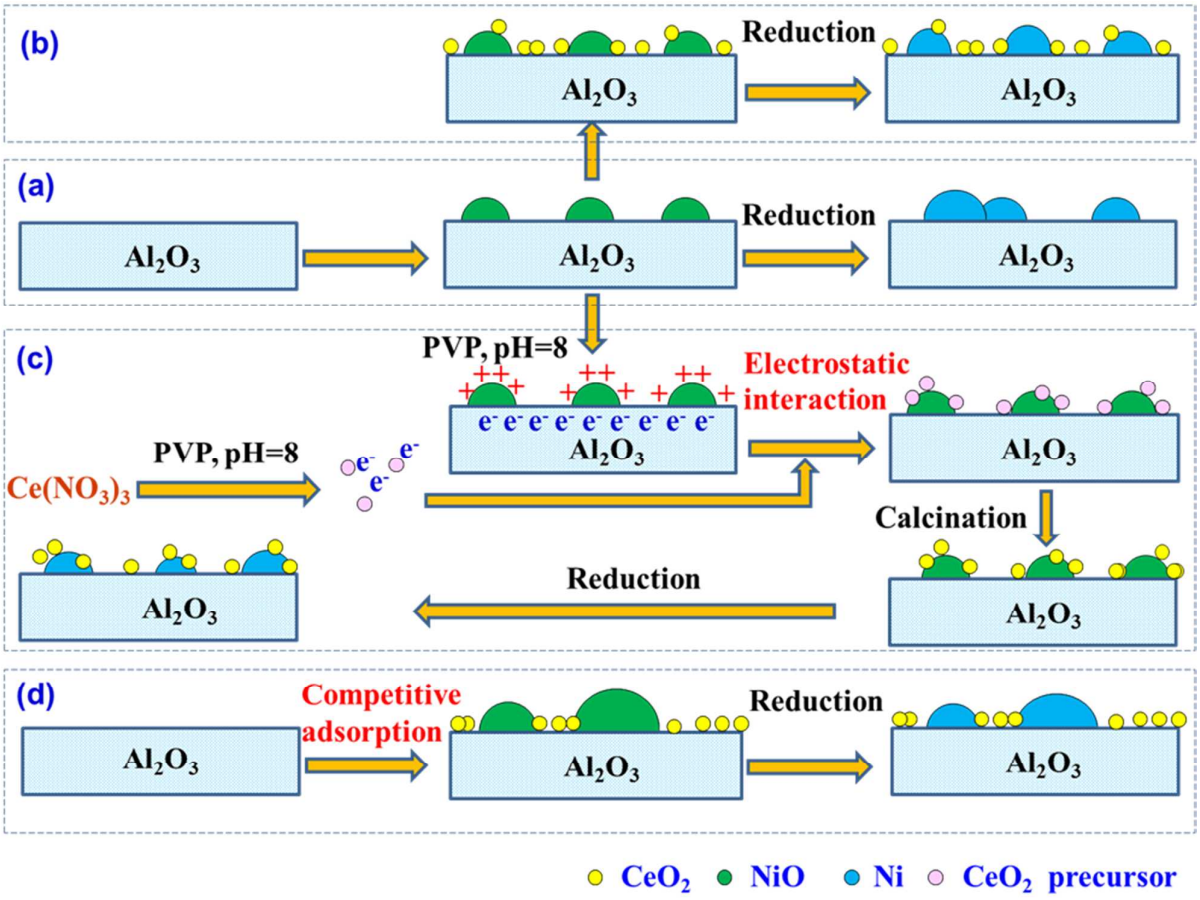

Fig. 7